Mechanisms and kinetics of amyloid aggregation investigated by a phenomenological coarse-grained model

Andrea Magno, Riccardo Pellarin, and Amedeo Caflisch

[1] *Department of Biochemistry, University of Zürich, Winterthurerstrasse 190, CH-8057, Zürich, Switzerland**

I. INTRODUCTION

Amyloid fibrils are ordered polypeptide aggregates that have been implicated in several neurodegenerative pathologies, such as Alzheimer's, Parkinson's, Huntington's and prion diseases[1,2], and, more recently, also in biological functionalities[3–5]. These findings have paved the way for a wide range of experimental and computational studies aimed at understanding the details of the fibril formation mechanism. Computer simulations using low-resolution models, which employ a simplified representation of protein geometry and energetics, have provided insights into the basic physical principles underlying protein aggregation in general[6–8] and ordered amyloid aggregation[9–15]. For example, Dokholyan and coworkers have used the Discrete Molecular Dynamics method[16,17] to shed light on the mechanisms of protein oligomerization[18] and the conformational changes that take place in proteins before the aggregation onset[19,20]. One challenging observation, which is difficult to observe by computer simulations, is the wide range of aggregation scenarios emerging from a variety of biophysical measurements[21,22]. Atomistic models have been employed to study the conformational space of amyloidogenic polypeptides in the monomeric state[23–25], the very initial steps of amyloid formation[26–32], and the structural stability of fibril models[33–35]. However, all-atom simulations of the kinetics of fibril formation are beyond what can be done with modern computers.

To overcome such computational limitations, simplified models have been developed and used to investigate the kinetics and pathways of oligomerization and fibril formation at different levels of resolution[36]. In this chapter we first review briefly the simplified models of aggregation. We then present our coarse-grained phenomenological (CGF) model of an amphipathic peptide[37], and its use for studying kinetics and thermodynamics, both in bulk conditions and in presence of other simplified (macro)molecules.

II. COARSE-GRAINED MODELS

In coarse-grained models, the complexity of a system (and therefore the computational cost) is reduced by grouping atoms into larger units or "beads", whose mutual interactions are usually approximated by a potential of mean force[38]. Several coarse-grained models of different resolutions have been developed to study aggregation (see Fig.1). Zhang and Muthukumar[39] have created a cuboid model able of reproducing the features of a nucleation-limited aggregation process. With their so-called "tube" model, Auer and coworkers[40] have shed light upon the conversion of a disordered aggregate into

an aggregating nucleus. Higher resolution models like the one developed by Thirumalai and collaborators[41] or the PRIME model of Nguyen and Hall[42] have also showed disordered aggregates in the early steps of aggregation. Several aggregation scenarios have been described with the three-bead model of Shea and coworkers[43]. In their model, the variation of a parameter related to the dihedral flexibility is able to reproduce different aggregation kinetics and metastable intermediates (amorphous and β-barrel like), which is in part similar to the CGF model[37]. The main difference between the Shea and CGF models is that the former is based on a coarse-graining from an atomistic description (i.e., "bottom-up" development), whereas the CGF model is purely phenomenological ("top-down") as explained in the next section.

III. THE CGF (COARSE-GRAINED PHENOMENOLOGICAL) MODEL

The coarse-grained model of an amphipathic peptide developed for studying aggregation kinetics and thermodynamics is a compromise between mesoscopic detail and computational efficiency. It must be stressed that this simplified model does not represent a particular protein sequence, i.e., it has not been generated by grouping into larger beads the atomic structure of a given (poly)peptide. It rather was designed from scratch for emulating the main experimental findings on fibril formation kinetics.

The peptide is approximated by 10 spherical beads, four of which represent the "backbone" (small beads) and six the "side chain" (large beads) (Fig. 2, top). The "backbone" beads carry partial charges of $\pm 0.4e$, thereby generating two dipoles; this part of the monomer is designed to interact specifically by intermolecular dipole-dipole interactions. The large beads interact only by van der Waals forces. The non-bonding interaction cut-off is set equal to 20 Å. The monomer displays an amphipathic moment, since eight of the ten beads have less favorable van der Waals interactions than the remaining two beads (black spheres in Fig. 2, top). The amphipathicity of the "molecule" allows the formation of amorphous aggregate, such as micellar oligomers, and the assembly of fibrils. In both of these types of aggregates, the hydrophobic spheres are buried and the hydrophilic spheres are exposed. The micellar oligomers are spherical and fluid-like, while the fibrils are ordered and rigid (see below).

The monomer can change its conformation by rotating around the internal dihedral defined by the small beads (Fig. 2, bottom). Using a one-dimensional spline function[44], a dihedral potential was designed with only two minima separated by a barrier (see Fig. 3). The only parameter that rules the relative populations of the amyloid-prone and amyloid-

protected states is the energy difference $dE = E_\pi - E_\beta$ between the conformation with perpendicular dipoles (E_π), which prevents ordered aggregation, and the conformation with parallel dipoles, which is prone to form fibrils (E_β). The use of a single parameter to model a complex process was inspired by the work of Zhou and Karplus, who have analyzed the folding kinetics of a model protein by varying a single parameter and shown that it is possible to recover several folding scenarios[45].

IV. AGGREGATION OF THE CGF PEPTIDE MODEL IN BULK SOLUTION

Unless specified explicitly, simulations are started from 125 monodispersed monomers of the CGF peptide in a cubic box with a size of 290 Å, corresponding to a concentration of 8.5 mM. After minimization and equilibration, simulations are performed with Langevin dynamics at 310 K with a very small friction coefficient of 0.01 ps^{-1} using CHARMM[46].

A. Aggregation kinetics and pathways

The range of aggregation kinetics of the CGF model is shown in Fig. 4, where the normalized degree of polymerization as a function of time is plotted for different values of the amyloidogenic propensity dE. The extent of aggregation is controlled by counting the number of polar contacts: a polar contact is formed whenever two dipoles of different monomers are closer than 5 Å. Three different kinetic phases are visible: lag, elongation, and final monomer-fibril equilibrium. The variable length of the lag phase and the higher heterogeneity at longer lag times are indicative of a stochastic nucleation[48]. Fibril formation is much slower for the β-unstable models (dE = -2.5 and -2.25 kcal/mol) than the β-stable models (dE = -1.0 and 0.0 kcal/mol). Both the lag phase and the elongation kinetics are affected by the single free parameter dE of the CGF model. Interestingly, the kinetics of aggregation are qualitatively consistent with the experimental data on single-point mutants of Aβ_{40} (Ref.[49]), which have shown that the β-sheet propensity and hydrophobicity affect the features of the aggregation process. This comparison shows that although the CGF model does not represent any particular polypeptide sequence, variations of the single parameter dE emulate the behavior observed for (slightly) different amyloidogenic sequences. Moreover, the anticorrelation between the length of the lag phase and the rapidity of the fibril elongation has also been observed experimentally on several samples prepared from amyloidogenic (poly)peptide sequences[47].

The distribution function $p(N)$ of the oligomer size N evaluated at the lag phase or

at the final equilibrium is depicted in Fig. 5. The monomer peak ranges from $N = 1$ to $N = 7$, the micellar peak from $N = 8$ to $N = 60$, and the fibrillar peak from $N = 61$ to $N = 125$. The micellar peak is present for the dE = -2.5 kcal/mol model at the lag phase, but disappears at the final equilibrium, where the fibril and the monomers are the only co-existing species. For the β-stable potential $dE = 0.0$ kcal/mol, the micellar peak is not observed at any concentration value. Indeed, a comparison of the lag times with the times of micelle formation (Fig. 6) shows that the fibril formation kinetics of the β-unstable and β-stable models are, respectively, slower and faster than micelle formation. In fact, micelles are intermediates consisting mainly of monomers in the π state, whereas the polymerization of β-stable monomers directly yields fibrils.

This observation is confirmed also by the analysis of aggregation pathways[50]. A total of 100 Langevin dynamics simulations for different values of dE were clustered according to three progress variables: the size of the largest aggregate N_{la}, the number of monomers in the β-state within the largest aggregate N_{la}^{β}, and the number of protofilaments in the largest aggregate N_{la}^{pf}, where a protofilament is defined as a file of monomers with intermolecular dipolar interactions parallel with its axis. The aggregation state network (Fig. 7) is a graph in which the states and direct transitions observed during the Langevin dynamics simulations are displayed as nodes and links, respectively. Furthermore, the size of each node reflects the statistical weight of the corresponding state. Micellar oligomers (white nodes, $N_{la} \sim 20$, N_{la}^{pf}=0) and fibrils (red nodes, $N_{la} \sim 100$, N_{la}^{pf}=4) are the most populated states during the lag phase and the final equilibrium, respectively. Strikingly, a greater variety of aggregation mechanisms emerges for the poorly amyloidogenic CGF peptide model (see Fig. 7, bottom) than the highly amyloidogenic CGF peptide model (see Fig. 7, top). Indeed, the former shows the presence of intermediates, i.e., protofibrils consisting of only two (green nodes) or three (blue nodes) protofilaments. According to this analysis, it is reasonable to expect that a mutation that decreases the β-aggregation tendency could result in a greater variety of prefibrillar aggregates, as in the case of the Arctic mutant (E22G) of the Alzheimer's Aβ peptide and the A30P mutant for α-synuclein, for which a more pronounced *in vitro* formation of oligomers and protofibrils was observed[51,52].

B. Mechanism of nucleation

The nucleation properties of the CGF model are investigated by evaluating the probability of fibril formation for β-subdomains, i.e., the clusters of interacting β-monomers.

The nucleus, defined as the oligomer containing a β-subdomain with a 50% probability to form a fibril, shows an increasing size upon destabilization of the β-state. Significantly different nucleation mechanisms are observed upon variation of the amyloidogenicity parameter dE (Fig. 8). For high values of the amyloidogenic propensity ($-2.0 \leq dE \leq 0.0$ kcal/mol), the nucleus size is sub-micellar, and nucleation is simply the aggregation of monomers in the β-state. On the contrary, for poorly amyloidogenic peptides, nucleus formation requires either spatial proximity of several monomers in the β-state (dE = -2.25 kcal/mol) within a micelle or collision of two peptide micelles with merging of their β-subdomains (dE = -2.5 kcal/mol). The variety of aggregation scenarios is also observed experimentally. An unstructured peptide with a marginally stable β-prone state like Aβ_{40} (Ref.[53,54]) visits oligomeric intermediates in the lag phase, and has a very weak dependence of the elongation rate on concentration due to the monomer-micelle equilibrium. This mechanism corresponds to the nucleated conformational conversion proposed by Serio *et al.*[55]. On the other hand, a functional and non-pathological amyloid in mammalians[56] lacks on-pathway intermediates and corresponds to the highly amyloidogenic CGF peptide model. Once more, by varying the only free parameter dE of the CGF model, it is possible to describe the aggregation properties of a wide and diverse range of (poly)peptide sequences.

C. Concentration effects

The dE parameter of the CGF model has a strong influence on the concentration dependence of the fibril formation kinetics. In agreement with the above-mentioned mechanism of nucleation, CGF peptides poorly prone to aggregation nucleate only at concentration values larger than the critical concentration of peptide micelle formation, whereas CGF peptides with a high value of amyloidogenicity nucleate even at lower concentrations (Fig. 9, left). Furthermore, the dependence of the elongation rate on the concentration is only marginal at low amyloidogenic tendency (Fig. 9 (b)). The reduced concentration dependence originates from competitive polymerizations, i.e., the elongation of the fibril and the presence of micellar oligomers. This observation is a consequence of the monomer-micelle equilibrium of the CGF peptide model, which maintains a nearly constant concentration of isolated monomers[57].

D. Amyloid fibril polymorphism

Experiments based on electron and atomic force microscopy as well as solid-state NMR spectroscopy revealed that changing the samples conditions, such as the pH[59] or the cosolvent concentration[60], or introducing a mechanical perturbation[61,62] results in different amyloid fibril morphologies. Furthermore, even within the same sample, a number of coexisting morphologies can be detected[59,63]. Recently, it was observed that the CGF peptide model is able to generate fibrils with distinct morphologies[64]. Interestingly, the populations of the different morphologies are strongly and nontrivially influenced by the amyloidogenic propensity dE, and two main mechanisms for fibril morphogenesis emerge. When the CGF peptide is highly prone to aggregate (dE = -1.5, -2.0 kcal/mol), the morphogenesis is under thermodynamic control, meaning that the morphology with the highest stability will emerge with the highest probability. In contrast, when the CGF peptide has a low amyloidogenic tendency (dE = -2.25, -2.5 kcal/mol), the fibril morphogenesis is under kinetic control. The morphologies that nucleate more readily are not necessarily the most stable ones, but those whose precursors are kinetically more accessible, as revealed by the free energy profiles of the fibrillation[64]. For the low amyloidogenic scenario, the process of morphology differentiation can be represented by a branched tree (Fig. 10). During the lag phase, the micellar oligomers are in equilibrium with the dispersed monomers. The early morphology differentiation occurs at the nucleation step, where the formation of the protofibrillar intermediates is regulated by the structural bifurcation of the nucleus. The 2PP and 3PP1 intermediates are competent to 4PF1 fibrils, while the 3PP2 intermediate is competent to 4PF2(+,-) fibrils. Alternatively, the presence of 3PP2+ and 3PP2- intermediates that are directly competent to 4PF2+ and 4PF2- fibrils, respectively, has been observed, although these pathways were not quantitatively analyzed. Finally, the pathway of formation of 4PF3 fibrils was not investigated in detail, due to the small number of nucleation events of this morphology. The multiple-pathways process observed here has a close similarity with the scenario described by Goldsbury *et al.*[65], where two different morphologies of Aβ have distinct maturation pathways, either with or without the presence of metastable protofibrils.

V. AGGREGATION IN THE PRESENCE OF LIPID VESICLES AND INERT CROWDERS

Amyloid aggregation *in vivo* does not occur in bulk solution. Rather, it takes place in the extracellular space, whose composition includes metabolites and proteins, or within the cell, which is usually densely occupied by (macro)molecules like proteins, nucleic acids, and polysaccharides, as well as macromolecular assemblies and organelles[66]. Several research groups have investigated the interactions between lipid vesicles and amyloid aggregates[67–69], whose accumulation on the surface of lipid bilayers was observed to cause membrane damage. Aggregation has also been studied in crowded media[70–72], where the thermodynamics and kinetics of aggregation are expected to sensibly change.

A. Effect of lipid bilayers on CGF peptide aggregation

A three-bead model of a lipid molecule has been developed to study the CGF peptide model aggregation kinetics in the presence of a lipid vesicle[73,74]. Several independent Langevin simulations at 310 K have been performed for four values of dE with 125 peptides initially monodispersed in a cubic box of length 290 Å and a preequilibrated unilamellar bilayer vesicle made up of 1000 lipids. Depending on the lipid/peptide van der Waals coupling parameter λ, between 50% and 80% of the CGF peptides are located on the lipid vesicle surface after the initial equilibration phase, i.e., before fibril formation (Table 1).

The effect of lipid bilayers on aggregation kinetics for different values of amyloidogenicity is reported in Table 2. Highly amyloidogenic peptides fibrillate more rapidly in the presence of lipid vesicles than in their absence, while the opposite is observed for peptides of low amyloidogenicity. The faster aggregation kinetics of highly amyloidogenic peptides is a consequence of their higher effective concentration on the lipid bilayer relative to the bulk. In contrast, despite the same increase of peptide concentration on the vesicle surface, fibrillation of peptides with low amyloidogenic propensity is slower in the presence of lipid vesicles. As mentioned in section III, peptides with low amyloidogenic potential can fibrillate only after aggregating into spherical oligomeric intermediates with hydrophobic interior and hydrophilic surface. In the simulations with lipids, such oligomeric intermediates form in the bulk but not on the vesicle. Fibrillation of low amyloidogenic peptides therefore takes place in the bulk and is slower than in the absence of a vesicle due to the lower effective concentration of peptides in the solvent. These simulation results are

consistent with and explain the apparently contradictory experimental observations on faster aggregation of the Aβ(Ref.[68]) or α-synuclein[75] peptides in the presence of lipid surfaces and slower aggregation of insulin (which has lower amyloidogenicity)[76], and have been confirmed by recent studies on the aggregation properties of human islet amyloid polypeptide hIAPP$_{1-19}$ in presence of lipid vesicles[77].

To investigate the influence of the CGF peptides on the lipid bilayer, the simulations were initiated with 20 spherical probes inside the vesicle. It was observed that leakage from the lipid vesicle is enhanced during fibril formation but not by the mature fibril[73]. More precisely, a comparison between the fibrillation and probe release rates (Fig. 11, left) revealed that probe release is fastest during fibril growth, whereas the kinetics of probe release in the presence of mature fibrils is as slow as in the absence of peptides, indicating that mature fibrils do not damage the integrity of the vesicle. Rather, the ongoing process of aggregation on the vesicle results in bilayer surface defects. This observation explains why for some amyloidogenic peptides there exist mutants that form fibrils more rapidly and are more toxic than the wild-type peptides, even though their fibrils are not toxic[78]. Moreover, these computational results are in agreement with the experiments performed by Engel *et al.* on membrane damage caused by human islet amyloid polypeptide fibril growth[69] (Fig. 11 right).

It has also been hypothesized that formation of toxic oligomers that induce membrane leakage could be the result of a backward production of oligomers from the mature fibril[79]. Interestingly, by modulating the attraction between the CGF peptides and the membrane, fibril disaggregation into soluble backwards oligomers has been observed[74]. The disaggregation process is driven by entropy and results in soluble protofibrillar oligomers. The protofibrillar oligomers are larger, more ordered, and more stable than those observed during the aggregation process and, importantly, are not detected in disaggregation simulations carried out in bulk solution, i.e., in the absence of lipid vesicles.

B. Effect of surfactants on CGF peptide aggregation

Surfactant molecules have been modeled using a similar three-bead model as that used for lipids. The surfactant model differs from lipid models used previously in two parameters (Table 1): the minimum of the van der Waals energy of the two hydrophobic beads is less favorable, and the radius of the hydrophilic bead is larger to enable the formation of amorphous aggregates. Using these parameters, the surfactant solution is not dominated by a micellar phase. Rather, the surfactants are organized either as

dispersed monomers or disordered aggregates[80].

In the absence of surfactants, all peptide models form fibrils within 1 μs without any discernible lag phase (Fig. 12, dotted lines). At a surfactant:peptide ratio of 8:1, the fibril formation kinetics of peptides with dE = -1.5 kcal/mol are almost unaffected, whereas already at a ratio of 4:1 the ordered self-assembly of peptides with $dE <$ -2.0 kcal/mol is significantly slower (Fig. 12, solid lines) mainly because of a longer lag phase. Moreover, for low-amyloidogenic peptides ($dE \leq$ -2.0 kcal/mol) no fibrillation is observed within the simulation length of 2 μs at a surfactant:peptide ratio of 8:1, but instead oligomers of $\sim$ 40 peptides form. These simulation results show that at a 4-fold molar excess of surfactant, the inhibition of fibrillation already depends strongly on the amyloidogenicity of the CGF peptide model.

C. Macromolecular crowding effect on CGF peptide aggregation

Simulations with the CGF peptide model together with softly repulsive spheres have been carried out to assess the influence on the aggregation kinetics of excluded volume and hindered peptide diffusion due to macromolecular crowding [81]. As in the case of lipid-bilayer vesicles, the net effect of macromolecular crowding crucially depends on the amyloidogenicity tendency of the CGF peptide. For peptides with low aggregation propensity, the self-association process is transition-state limited, where the kinetic bottleneck is the formation of the fibril nucleus. In this case, since the oligomers, including the nucleus, are thermodynamically favored (with respect to the isolated monomers) by the excluded volume effect, macromolecular crowding accelerates peptide assembly and has an effect analogous to that of an increase in peptide concentration (Fig. 13, left). This trend is analogous to that observed experimentally by Munishkina *et al.*, who have studied the effect of increasing the PEG concentration on the α-synuclein aggregation process[71].

On the other hand, when the aggregation mechanism is fast and proceeds directly from monomers to fibril, the process is diffusion limited, and the thermodynamic stabilization of oligomers is less important than the reduction in peptide mobility. In this case, the bottleneck is not the formation of the nucleus; the rate-limiting step for peptides that show a direct aggregation mechanism is the elongation of the fibril. Therefore, in this case macromolecular crowding is much less efficient in accelerating the self-association of peptides than an equivalent increase in peptide concentration, since the peptides diffusion is hindered by the crowders (Fig.13, right).

VI. CONCLUSION

Atomistic simulations of aggregation are limited by short time scale, while experimental approaches to amyloid fibril formation have insufficient spatial resolution. Coarse-grained models of polypeptide aggregation sacrifice atomistic detail to reach timescales that allow the comparison with and interpretation of experimental data. The models presented in this chapter have shed light upon amyloid aggregation kinetics and mechanisms, which is helpful to formulate a unified picture of the available experimental data.

The CGF model has only one tunable parameter, the difference dE between the energy of the amyloid-competent and the amyloid-protected state of the monomer[37]. Variations of this parameter reproduce several aggregation scenarios, both under homogeneous and heterogeneous conditions. It is important to highlight that the CGF model does not mimic any particular amyloid (poly)peptide sequence. However, the different aggregation kinetics obtained with this model can be directly compared with experiments carried out with specific proteins. In Table 3 are reviewed the principal characteristics of the aggregation process for both the high and low amyloidogenic tendency, and in both cases several examples of real amyloid-forming (poly)peptide sequences are listed. It is important to note that (coarse-grained) simulations, e.g., those with the CGF[37] and Shea[43] models, allow for the emulation of conditions and/or phenomena that are not accessible by (standard) experiments. As an example, the possibility to change solely the intrinsic conformational landscape of a monomer without affecting the inter-monomer interactions is an advantage of the (coarse-grained) simulation methods with respect to conventional experimental techniques such as mutagenesis and solvent-induced conformational changes, by which it is not possible to decouple changes in intra from inter-molecular interactions.

In conclusion, a slight modification of the free energy profile of an extremely simplified model of an amphipathic peptide is sufficient to observe a wide range of different fibril formation mechanisms, providing a unifying description of the heterogeneity of the experimentally observed kinetics of amyloid fibril formation.

---

* Author to whom correspondence should be addressed: caflisch@bioc.uzh.ch

[1] C. M. Dobson, Protein Folding and Misfolding. *Nature*, **426**, 884-890 (2003).

[2] P. T. Lansbury, H. A. Lashuel, A century-old debate on protein aggregation and neurodegeneration enters the clinic. *Nature*, **443**, 774-779 (2006).

[3] D. M. Fowler, A. V. Koulov, W. E. Balch, J. W. Kelly, Functional amyloid–from bacteria to

humans. *Trends Biochem. Sci.*, **32**, 217-224 (2007).

[4] S. K. Maji, M. H. Perrin, M. R. Sawaya, S. Jessberger, K. Vadodaria, R. A. Rissman, P. S. Singru, K. P. R. Nilsson, R. Simon, D. Schubert *et al.*, Functional amyloids as natural storage of peptide hormones in pituitary secretory granules. *Science*, **325**, 328-332 (2009).

[5] J. Greenwald, R. Riek, Biology of amyloid: structure, function, and regulation. *Structure*, **18**, 1244-1260 (2010).

[6] R. A. Broglia, G. Tiana, S. Pasquali, H. E. Roman, E. Vigezzi, Folding and aggregation of designed proteins. *Proc. Natl Acad. Sci.* USA, **95**, 12930-12933 (1998).

[7] P. Gupta, C. K. Hall, A. C. Voegler, Effect of denaturant and protein concentrations upon protein refolding and aggregation: a simple lattice model. *Protein Sci.*, **7**, 2642-2652 (1998).

[8] P. M. Harrison, H. S. Chan, S. B. Prusiner, F. E. Cohen, Thermodynamics of model prions and its implications for the problem of prion protein folding. *J. Mol. Biol.*, **286**, 593-606 (1999).

[9] B. Urbanc, L. Cruz, S. Yun, S. V. Buldyrev, G. Bitan, D. B. Teplow, H. E. Stanley, In silico study of amyloid beta-protein folding and oligomerization. *Proc. Natl Acad. Sci.* USA, **101**, 17345-17350 (2004).

[10] J. Sørensen, X. Periole, K. K. Skeby, S. -J. Marrink, B. Schiøtt, Protofibrillar Assembly Toward the Formation of Amyloid Fibrils. *J. Chem. Phys. Lett.*, **2**, 2385-2390 (2011).

[11] H. Jang, C. K. Hall, Y. Zhou, Assembly and kinetic folding pathways of a tetrameric beta-sheet complex: molecular dynamics simulations on simplified off-lattice protein models. *Biophys. J.*, **86** (1 Pt 1), 31-49 (2004).

[12] R. I. Dima, D. Thirumalai, Exploring protein aggregation and self-propagation using lattice models: phase diagram and kinetics. *Protein Sci.*, **11** (5), 1036-1049 (2002).

[13] E. Malolepsza, M. Boniecki, A. Kolinski, L. Piela, Theoretical model of prion propagation: a misfolded protein induces misfolding. *Proc. Natl Acad. Sci.* USA, **102**, 7835-7840 (2005).

[14] S. D. Khare, F. Ding, K. N. Gwanmesia, N. V. Dokholyan, Molecular origin of polyglutamine aggregation in neurodegenerative diseases. *PLoS Comput. Biol.*, **1**, 230-235 (2005).

[15] Y. Chen, N. V. Dokholyan, A single disulfide bond differentiates aggregation pathways of beta2-microglobulin. *J. Mol. Biol.*, **354**, 473-482 (2005).

[16] N. V. Dokholyan, S. V. Buldyrev, H. E. Stanley, E. I. Shakhnovich, Discrete molecular dynamics studies of the folding of a protein-like model. *Folding Des.*, **3**, 577587 (1998).

[17] F. Ding, S. V. Buldyrev, N. V. Dokholyan, Folding Trp-cage to NMR resolution native structure using a coarse-grained protein model. *Biophys. J.*, **88**, 147155 (2005).

[18] F. Ding, N. V. Dokholyan, S. V. Buldyrev, H. E. Stanley, E. I. Shakhnovic, Molecular

dynamics simulation of the SH3 domain aggregation suggests a generic amyloidogenesis mechanism. *J. Mol. Biol.*, **324**, 851-857 (2002).

[19] F. Ding, J. M. Borreguero, S. V. Buldyrey, H. E. Stanley, N. V. Dokholyan, Mechanism for the alpha-helix to beta-hairpin transition. *Proteins*, **53**, 220-228 (2003).

[20] F. Ding, J. J. LaRocque, N. V. Dokholyan, Direct observation of protein folding, aggregation, and a prion-like conformational conversion. *J. Biol. Chem.*, **48**, 40235-40240 (2005).

[21] W. S. Gosal, I. J. Morten, E. W. Hewitt, D. A. Smith, N. H. Thomson, S. E. Radford, Competing pathways determine fibril morphology in the self-assembly of beta2-microglobulin into amyloid. *J. Mol. Biol.*, **351**, 850-864 (2005).

[22] G. Plakoutsi, F. Bemporad, M. Calamai, N. Taddei, C. M. Dobson, F. Chiti, Evidence for a mechanism of amyloid formation involving molecular reorganisation within native-like precursor aggregates. *J. Mol. Biol.*, **351**, 910-922 (2005).

[23] A. Vitalis, X. Wang, R. V. Pappu, Quantitative characterization of intrinsic disorder in polyglutamine: insights from analysis based on polymer theories. *Biophys. J.*, **93**, 1923-1937 (2007).

[24] A. Vitalis, N. Lyle, R. V. Pappu, Thermodynamics of beta-sheet formation in polyglutamine. *Biophys. J.*, **97**, 303-311 (2009).

[25] A. Vitalis, A. Caflisch, Micelle-like architecture of the monomer ensemble of Alzheimer's amyloid- peptide in aqueous solution and its implications for Aβ aggregation. *J. Mol. Biol.*, **403**, 148-165 (2010).

[26] J. Gsponer, U. Haberthr, A. Caflisch, The role of side-chain interactions in the early steps of aggregation: Molecular dynamics simulations of an amyloid-forming peptide from the yeast prion Sup35. *Proc. Natl. Acad. Sci.* USA, **100**, 5154-5159 (2003).

[27] W. Hwang, S. Zhang, R. D. Kamm, M. Karplus, Kinetic control of dimer structure formation in amyloid fibrillogenesis. *Proc. Natl. Acad. Sci.* USA, **101**, 12916-12921 (2004).

[28] M. L. de la Paz, G. M. S. de Mori, L. Serrano, G. Colombo, Sequence dependence of amyloid fibril formation: insights from molecular dynamics simulations. *J. Mol. Biol.*, **349**, 583-596 (2005).

[29] M. Cecchini, R. Curcio, M. Pappalardo, R. Melki, A. Caflisch, A molecular dynamics approach to the structural characterization of amyloid aggregation. *J. Mol. Biol.*, **357**, 1306-1321 (2006).

[30] B. Strodel, C. S. Whittleston, D. J. Wales, Thermodynamics and kinetics of aggregation for the GNNQQNY peptide. *J. Am. Chem. Soc.*, **129**, 16005-16014 (2007).

[31] A. De Simone, L. Esposito, C. Pedone, L. Vitagliano, Insights into stability and toxicity of

amyloid-like oligomers by replica exchange molecular dynamics analyses. *Biophys. J.*, **95**, 1965-1973 (2008).

[32] G. Bellesia, J. -E. Shea, What determines the structure and stability of KFFE monomers, dimers, and protofibrils? *Biophys. J.*, **96**, 875-886 (2009).

[33] B. Ma, R. Nussinov, Stabilities and conformations of Alzheimer's beta -amyloid peptide oligomers (Abeta 16-22, Abeta 16-35, and Abeta 10-35): Sequence effects. *Proc. Natl. Acad. Sci.* USA, **99**, 14126-14131 (2002).

[34] N. -V. Buchete, R. Tycko, G. Hummer, Molecular dynamics simulations of Alzheimer's beta-amyloid protofilaments. *J. Mol. Biol.*, **353**, 804-821 (2005).

[35] C. Wu, M. T. Bowers, J. -E. Shea, Molecular structures of quiescently grown and brain-derived polymorphic fibrils of the Alzheimer amyloid abeta9-40 peptide: a comparison to agitated fibrils. *PLoS Comput. Biol.*, **6**, e1000693 (2010).

[36] C. Wu, J. -E. Shea, Coarse-grained models for protein aggregation. *COSB*, **21**, 209-220 (2011).

[37] R. Pellarin, A. Caflisch, Interpreting the aggregation kinetics of amyloid peptides. *J. Mol. Biol.*, **360**, 882-892 (2006).

[38] M. Müller, K. Katsov, M. Schick, Biological and synthetic membranes: What can be learned from a coarse-grained decription? *Physics Reports*, **434**, 113-176 (2006).

[39] J. Zhang, M. Muthukumar, Simulations of nucleation and elongation of amyloid fibrils. *J. Chem. Phys.*, **130**, 035102 (2009).

[40] S. Auer, C. M. Dobson, M. Vendruscolo, A. Maritan, Self-templated nucleation in peptide and protein aggregation. *PLos Comput. Biol.*, **4**, e1000222 (2008).

[41] M. S. Li, D. K. Klimov, J. E. Straub, D. Thirumalai, Probing the mechanisms of fibril formation using lattice models. *J. Chem. Phys*, **129**, 175101 (2008).

[42] H. D. Nguyen, C. K. Hall, Molecular dynamics simulations of spontaneous fibril formation by random-coil peptides. *Proc. Natl Acad. Sci.* USA, **101**, 16180-16185 (2004).

[43] G. Bellesia, J. -E. Shea, Self-assembly of beta-sheet forming peptides into chiral fibrillar aggregates. *J. Chem. Phys.*, **126**, 245104 (2007).

[44] A. D. J. MacKerell, M. Feig, C. L. Brooks, Improved treatment of the protein backbone in empirical force fields. *J. Am. Chem. Soc.*, **126**, 698-699 (2004).

[45] Y. Zhou. M. Karplus, Interpreting the folding kinetics of helical proteins. *Nature*, **401**, 400-403 (1999).

[46] B. R. Brooks, C. L. Brooks, A. D. Mackerell, L. Nilsson, R. J. Petrella, B. Roux, Y. Won, G. Archontis, C. Bartels, S. Boresch *et al.*, CHARMM: the biomolecular simulation program *J*

Comput. Chem., **30**, 1545-1614 (2009).

[47] M. Fändrich, Absolute correlation between lag time and growth rate in the spontaneous formation of several amyloid-like aggregates and fibrils. *J. Mol. Biol.*, **365**, 1266-1270 (2007).

[48] P. Hortschansky, V. Schroeckh, T. Christopeit, G. Zandomeneghi, M. Fändrich, The aggregation kinetics of Alzheimer's beta-amyloid peptide is controlled by stochastic nucleation. *Protein Sci.*, **14**, 1753-1759 (2005).

[49] T. Christopeit, P. Hortschansky, V. Schroeckh, K. Guhrs, G. Zandomeneghi, .M Fändrich, Mutagenic analysis of the nucleation propensity of oxidized Alzheimer's beta-amyloid peptide. *Protein Sci.*, **14**, 2125-2131 (2005).

[50] R. Pellarin, E. Guarnera, A. Caflisch, Pathways and intermediates of amyloid fibril formation. *J. Mol. Biol.*, **374**, 917-924 (2007).

[51] C. Nilsberth, A. Westlind-Danielsson, C. B. Eckman, M. M. Condron, K. Axelman, C. Forsell *et al.*, The 'Arctic' APP mutation (E693G) causes Alzheimer's disease by enhanced Abeta protofibril formation. *Nature Neurosci.*, **4**, 887-893 (2001).

[52] K. A. Conway, S. J. Lee, J. C. Rochet, T. T. Ding, R. E. Williamson, P. T. Lansbury, Acceleration of oligomerization, not fibrillization, is a shared property of both alpha-synuclein mutations linked to early-onset Parkinson's disease: implications for pathogenesis and therapy. *Proc. Natl Acad. Sci.* USA, **97**, 571-576 (2000).

[53] R. Sabate, J. Estelrich, Evidence of the existence of micelles in the fibrillogenesis of beta-amyloid peptide. *J. Phys. Chem. B*, **109**, 11027-11032 (2005).

[54] A. Lomakin, D. S. Chung, G. B. Benedek, D. A. Kirschner, D. B. Teplow, On the nucleation and growth of amyloid beta-protein fibrils: detection of nuclei and quantitation of rate constants. *Proc. Natl Acad. Sci.* USA, **93**, 1125-1129 (1996).

[55] T. R. Serio, A. G. Cashikar, A. S. Kowal, G. J. Sawicki, J. J. Moslehi, L. Serpell *et al.*, Nucleated conformational conversion and the replication of conformational information by a prion determinant. *Science*, **289**, 1317-1321 (2000).

[56] D. M. Fowler, A. V. Koulov, C. Alory-Jost, M. S. Marks, W. E. Balch, J. W. Kelly, Functional amyloid formation within mammalian tissue. *PLoS Biol.*, **4**, e6 (2006).

[57] A. Lomakin, D. B. Teplow, D. A. Kirschner, G. Benedek, Kinetic theory of fibrillogenesis of amyloid beta-protein. *Proc. Natl Acad. Sci.* USA, **94**, 7942-7947 (1997).

[58] L. Nielsen, R. Khurana, A. Coats, S. Frokjaer, J. Brange, S. Vyas, V. N. Uversky, A. L. Fink, Effect of environmental factors on the kinetics of insulin fibril formation: elucidation of the molecular mechanism. *Biochemistry*, **40**, 6036-6046 (2001).

[59] C. Wasmer, A. Soragni, R. Sabate, A. Lange, R. Riek, B. H. Meier, Infectious and nonin-

fectious amyloids of the HET-s(218-289) prion have different NMR spectra. *Angew. Chem.*, Int. Ed., **47**, 5839-5841 2008.

[60] W. Dzwolak, S. Grudzielanek, V. Smirnovas, R. Ravindra, C. Nicolini, R. Jansen, A. Loksztejn, S. Porowski, R. Winter, Ethanol-perturbed amyloidogenic self-assembly of insulin: looking for origins of amyloid strains. *Biochemistry*, **44**, 8948-8958 (2005).

[61] A. T. Petkova, R. D. Leapman, Z. Guo, W. -M. Yau, M. P. Mattson, R. Tycko, Self-propagating, molecular-level polymorphism in Alzheimer's beta-amyloid fibrils. *Science*, **307**, 262-265 (2005).

[62] A. K. Paravastu, A. T. Petkova, R. Tycko, Polymorphic fibril formation by residues 10-40 of the Alzheimer's beta-amyloid peptide. *Biophys. J.*, **90**, 4618-4629 (2006).

[63] J. Meinhardt, C. Sachse, P. Hortschansky, N. Grigorieff, M. Fändrich, Abeta(1-40) fibril polymorphism implies diverse interaction patterns in amyloid fibrils. *J. Mol. Biol.*, **386**, 869-877 (2009).

[64] R. Pellarin, P. Schuetz, E. Guarnera, A. Caflisch, Amyloid fibril polymorphism is under kinetic control. *J. Am. Chem. Soc.*, **132**, 14960-14970 (2010).

[65] C. Goldsbury, P. Frey, V. Olivieri, U. Aebi, S. A. Müller, Multiple assembly pathways underlie amyloid-beta fibril polymorphisms. *J. Mol.Biol.*, **352**, 282-298 (2005).

[66] J. R. Ellis, Macromolecular crowding: obvious but underappreciated. *Trends Biochem. Sci.* **26**, 597-604 (2001).

[67] D. Lopes, A. Meister, A. Gohlke, A. Hauser, A. Blume, R. Winter, Mechanism of islet amyloid polypeptide fibrillation at lipid interfaces studied by infrared reflection absorption spectroscopy. *Biophys. J.*, **93**, 3132-3141 (2007).

[68] E. Chi, C. Ege, A. Winans, J. Majewski, G. Wu, K. Kjaer, K. Lee, Lipid membrane templates the ordering and induces the fibrillogenesis of Alzheimer's disease amyloid-beta peptide. *Proteins*, **72**, 1-24 (2008).

[69] M. F. M. Engel, L. Khemtémourian, C. Kleijer, H. Meeldijk, J. Jacobs, A. Verkleij *et al.*, Membrane damage by human islet amyloid polypeptide through fibril growth at the membrane. *Proc. Natl Acad. Sci. USA*, **105**, 60336038 (2008).

[70] R. J. Ellis, A. P. Minton, Protein aggregation in crowded environments. *Biol. Chem.*, **387**, 485-497 (2006).

[71] L. A. Munishkina, E. M. Cooper, V. N. Uversky, A. L. Fink, The effect of macromolecular crowding on protein aggregation and amyloid fibril formation. *J. Mol. Recognit.*, **17**, 456-464 (2004).

[72] L. A. Munishkina, A. Ahmad, A. L. Fink, V. N. Uversky, Guiding protein aggregation with

macromolecular crowding. *Biochemistry* **47**, 8993-9006 (2008).

[73] R. Friedman, R. Pellarin, A. Caflisch, Amyloid aggregation on lipid bilayers and its impact on membrane permeability. *J. Mol. Biol.*, **387**, 407-415 (2009).

[74] R. Friedman, R. Pellarin, A. Caflisch, Soluble Protofibrils as Metastable Intermediates in Simulations of Amyloid Fibril Degradation Induced by Lipid Vesicles *J. Phys. Chem. Lett.*, **1**, 471-474 (2010).

[75] M. J. Volles, S. J. Lee, J. C. Rochet, M. D. Shtilerman, T. T. Ding, J. C. Kessler, P. T. Lansbury, Vesicle permeabilization by protofibrillar alpha-synuclein: implications for the pathogenesis and treatment of Parkinson's disease. *Biochemistry*, **40**, 7812-7819 (2001).

[76] J. Sharp, J. Forrest, R. Jones, Surface denaturation and amyloid fibril formation of insulin at model lipid-water interfaces. *Biochemistry*, **41**, 15810-15819 (2002).

[77] L. Khemtémourian, M. F. M. Engel, R. M. J. Liskamp, J. W. M. Höppener, J. A. Killian, The N-terminal fragment of human islet amyloid polypeptide is non-fibrillogenic in the presence of membranes and does not cause leakage of bilayers of physiologically relevant lipid composition. *Biochimica et Biophysica Acta-Biomembranes*, **1798**, 1805-1811 (2010).

[78] H. Lashuel, P. Lansbury, Are amyloid diseases caused by protein aggregates that mimic bacterial pore-forming toxins? *Q. Rev. Biophys.*, **39**, 167-201 (2006).

[79] I. C. Martins, I. Kuperstein, H. Wilkinson, E. Maes, M. Vanbrabant, W. Jonckheere, P. V. Gelder, D. Hartmann, R. D'Hooge, B. D. Strooper *et al.*, Lipids revert inert Abeta amyloid fibrils to neurotoxic protofibrils that affect learning in mice. *EMBO J*, **27**, 224-233 (2008).

[80] R. Friedman, A. Caflisch, Surfactant Effects on Amyloid Aggregation Kinetics. *J. Mol. Biol.*, **414**, 303-312 (2011).

[81] A. Magno, A. Caflisch, R. Pellarin, Crowding Effects on Amyloid Aggregation Kinetics. *J. Phys. Chem. Lett.*, **1**, 3027-3032 (2010).

Type of molecule	$R_{hydrophilic}$ [nm]	$R_{hydrophobic}$ [nm]	$\epsilon_{hydrophilic}$ [kcal/mol]	$\epsilon_{hydrophobic}$ [kcal/mol]	λ^a	Fraction of CGF peptides bound to lipid vesicles	Reference
lipid	0.31	0.3	-0.1	-1.265	0.87-0.90	50%	[73]
lipid	0.31	0.3	-0.1	-1.265	0.95	80%	[74]
surfactant	0.35	0.3	-0.1	-0.8	1		[80]

TABLE 1. Three-bead lipid and surfactants models used with CGF peptide model. [a]Scaling factor for the vdW interactions between lipids or surfactants and peptides. Different scaling is used to model different systems, i.e., surfactants ($\lambda = 1$), moderately attractive ($\lambda \leq 0.9$) and strongly attractive ($\lambda \approx 0.95$) lipid bilayers.

Scaling of peptide/lipid interactions	Amyloido-genicity	Number of runs with fibril formation	Lag time t_{50} [ns] with membrane	without membrane
0.87	high	10/10	11 ± 1	19 ± 3
	interm.	29/29	89 ± 29	56 ± 15
	low	17/20	**958** ± 503	124 ± 28
	very low	0/10	> **2000**	318 ± 133
0.90	high	10/10	10 ± 1	19 ± 3
	interm.	30/30	69 ± 23	56 ± 15
	low	0/20	> **2000**	124 ± 28
	very low	0/20	> **2000**	318 ± 133

TABLE 2. Characteristic lag time of aggregation t_{50} for CGF peptide model for different amyloidogenic tendency in the presence or absence of lipid vesicles[73]. Values in boldface are significantly larger in the presence of the vesicles

high amyloidogenicity	low amyloidogenicity	Ref.
small nucleus	large nucleus	[37]
fast fibril formation	slow fibril formation	[37]
downhill	micellar intermediates	[37]
no intermediates	protofibrillar intermediates	[50]
single pathway	multiple pathways	[50]
strong concentration dependence	growth rate marginally dependent on concentration	[37]
polymorphism under thermodynamic control	polymorphism under kinetic control	[64]
can promote membrane leakage	does not promote membrane leakage	[73]
slightly accelerated by membranes	decelerated by membranes	[73]
marginally influenced by surfactants	decelerated by surfactants	[80]
not accelerated by macromolecular crowding	accelerated by macromolecular crowding	[81]
Phe-Phe, GNNQQNY, transthyretin, Aβ_{42}	Aβ_{40}, Sup35, prion protein, myoglobin	-

TABLE 3. Influence of amyloidogenic propensity on the aggregation kinetics and pathways of the CGF model[37]. The last line lists some examples but it must be stressed that amyloidogenic tendency strongly depends on external conditions, so that the same polypeptide sequence can show drastically different amyloidogenic tendency depending on pH, temperature, etc.

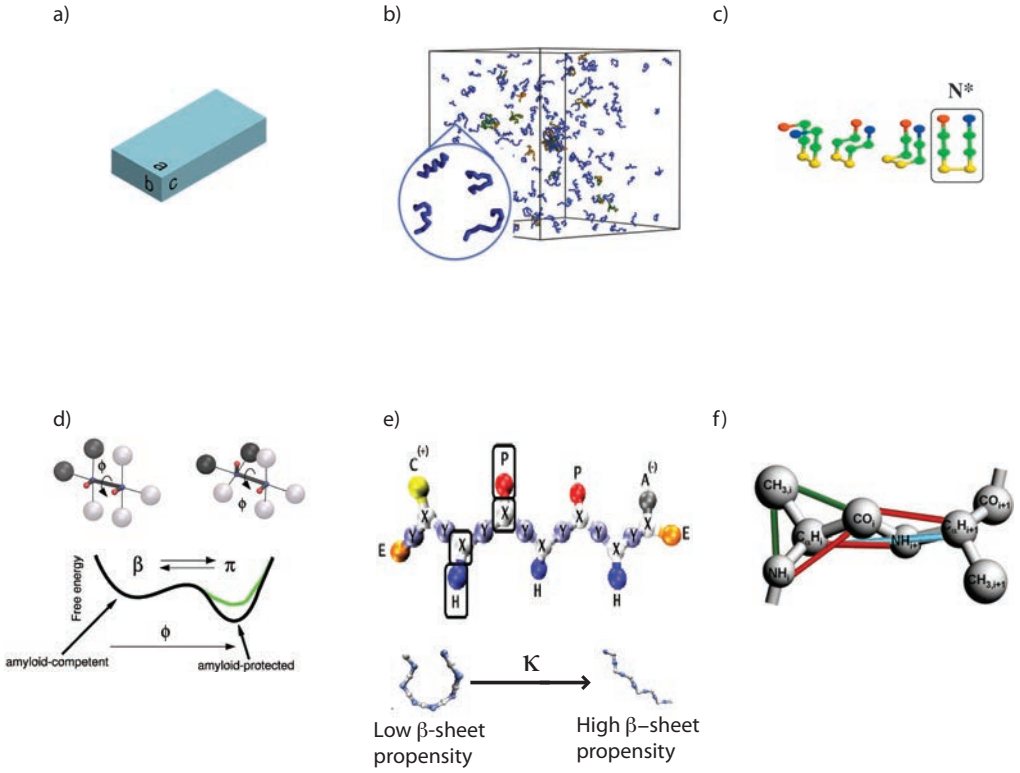

FIG. 1. Main coarse-grained models discussed in section II. a) Cuboid model[39]; b) tube model[40]; c) lattice model[41]; d) CGF model[37]; e) Shea model[43]; f) Hall model[42]. Reprinted from[36] with permission by Elsevier.

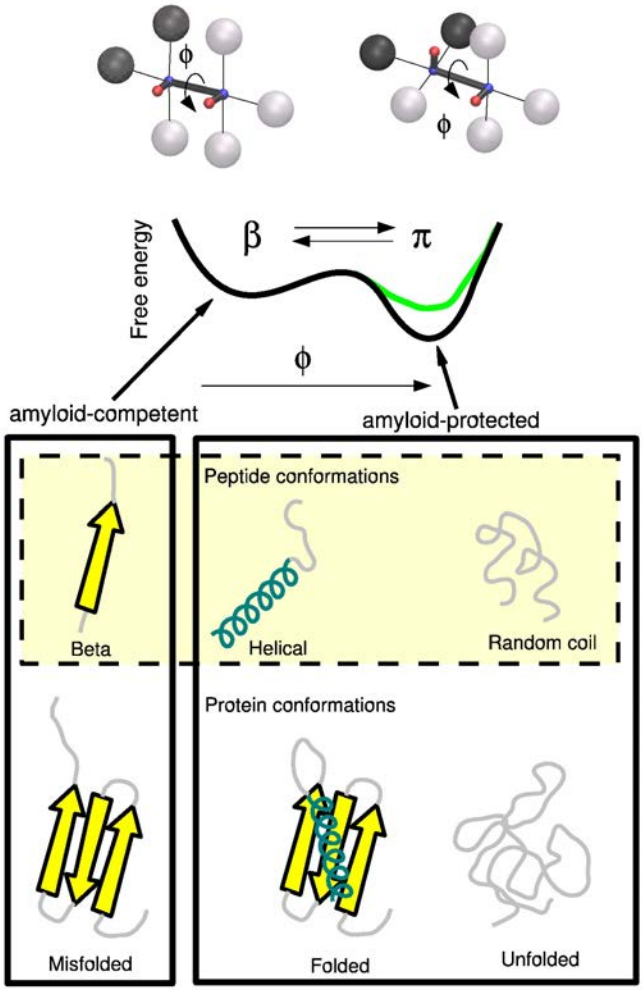

FIG. 2. The CGF model: sticks and beads representations of the monomer in the amyloid-competent state β and the amyloid-protected state π[37]. The large spheres are hydrophobic (black) and hydrophilic (gray), while the two dipoles are shown with small red and blue spheres. The size of the spheres does not represent the actual van der Waals radii, which are 2.5 Å for the black and gray spheres and 2.0 Å for the red and blue spheres. The β and π states of the monomer are shown on top of the two corresponding minima of the free energy, plotted as a function of the dihedral angle ϕ of the two dipoles. Reprinted from[50] with permission by Elsevier.

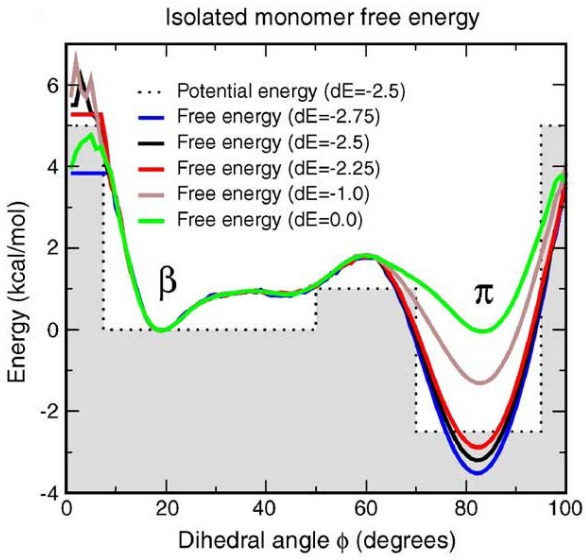

FIG. 3. The dotted line is the dihedral potential with a dE = -2.5 kcal/mol energy difference between amyloid-protected and amyloid-competent state. The five continuous lines represent the free energy profile of the isolated monomer for five different dihedral potentials. Since the peptide has only one degree of freedom, dE is close to the free-energy difference between the two aforementioned states. For instance, when dE = 0.0 kcal/mol, the π and β states are equally populated, whereas for dE = -1.5, -2.0, and -2.25 kcal/mol, the π state is about 15, 39, and 64 times more populated than the β state, respectively. Reprinted from[37] with permission by Elsevier.

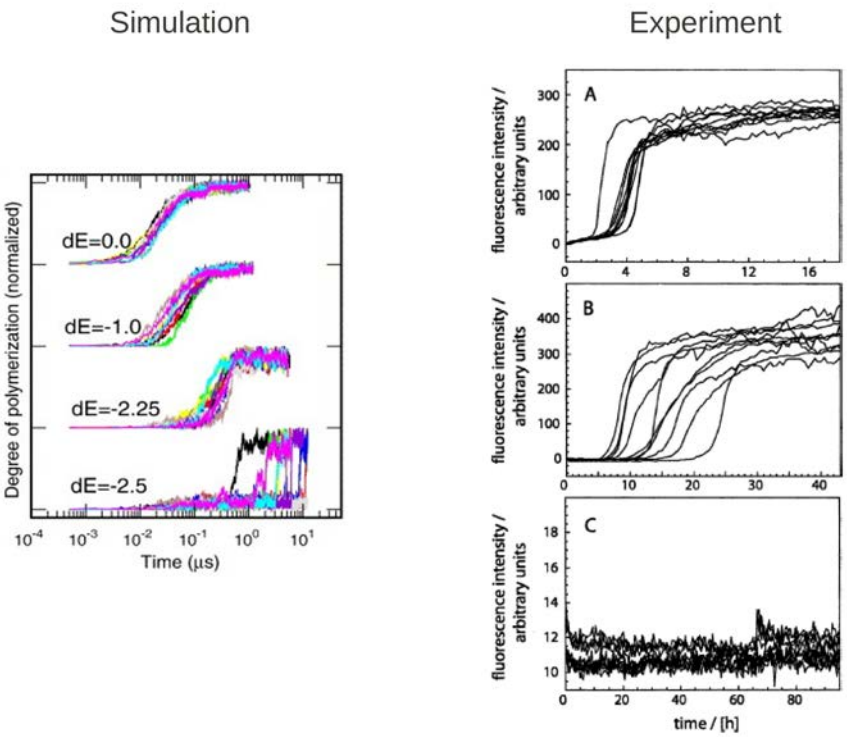

FIG. 4. Influence of amyloidogenic tendency on aggregation kinetics. (Left): Time series of the fraction of ordered aggregation evaluated at four values of the amyloidogenic tendency, from very prone to form fibrillar aggregates (dE = 0.0 kcal/mol) to marginal propensity (dE = -2.5 kcal/mol). Ten independent simulations are shown for each dE value. (Right): Fluorescence intensity (degree of aggregation) of V18I (a), V18Q (b) and V18P (c) mutants of Aβ_{40} (Ref.[49]). Note that the ns-μs timescales in the CGF model simulations are much shorter than in the experiments (hours) because of the much higher concentration in the former (8.5 mM) than in the latter (120 μM). Reprinted from[37] (left) and[49] (right) with permission by Elsevier (left) and Jon Wiley & Sons (right).

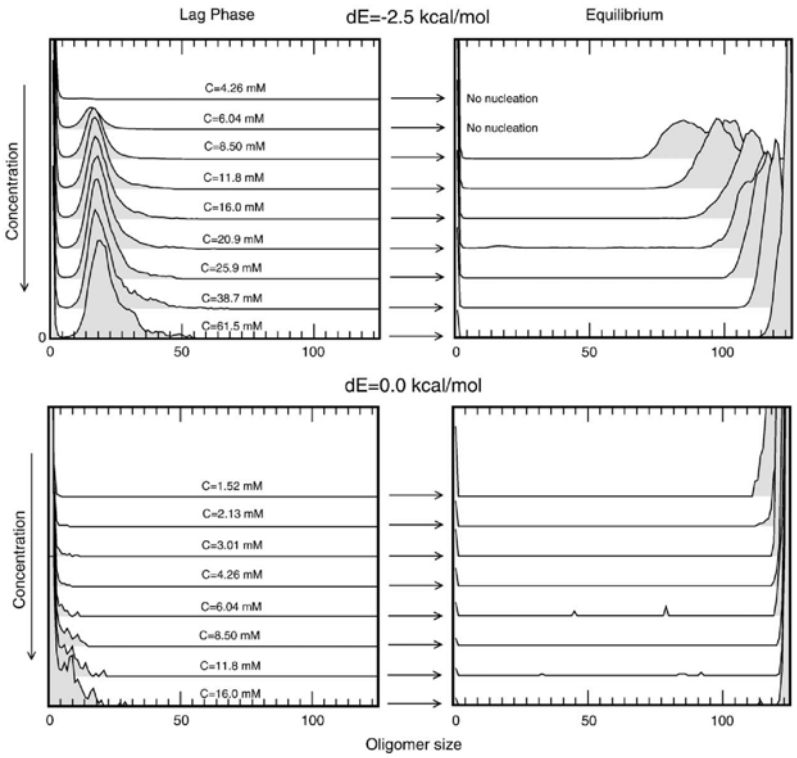

FIG. 5. Oligomer size histograms of the dE = -2.5 kcal/mol potential (top) and dE = 0.0 kcal/mol (bottom) calculated at the lag phase (left) and at the final equilibrium (right). The z-dimension represents the relative probability. Note that most of the results were obtained at a concentration C = 8.5 mM which is the lowest value at which fibril formation takes place within a reasonable simulation time for the dE = -2.5 kcal/mol model (10 μs in about 17 days on a single Xeon 5410 processor). Reprinted from[37] with permission by Elsevier.

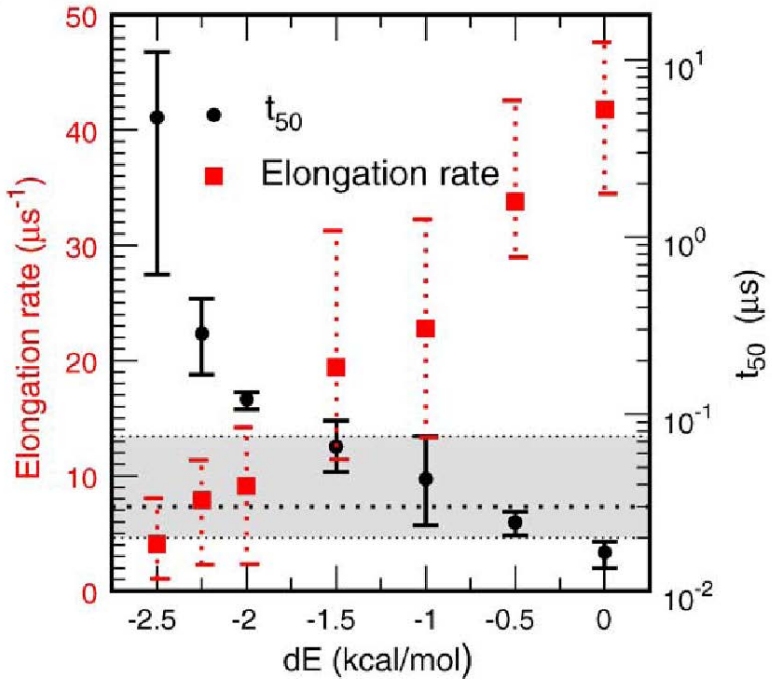

FIG. 6. Influence of the amyloidogenicity parameter dE on the kinetics of the CGF model. The time needed to reach 50% of the maximal amplitude t_{50} (black circles and y-axis legend on the right) and the elongation rate (red squares and y-axis legend on the left) are displayed for seven dE values. Symbols represent the average value of ten independent runs, and the error bars are the maximum and minimum values. The broken line and the gray band indicate the average and the maxmin values for the time of micelle formation, respectively. Reprinted from[37] with permission by Elsevier.

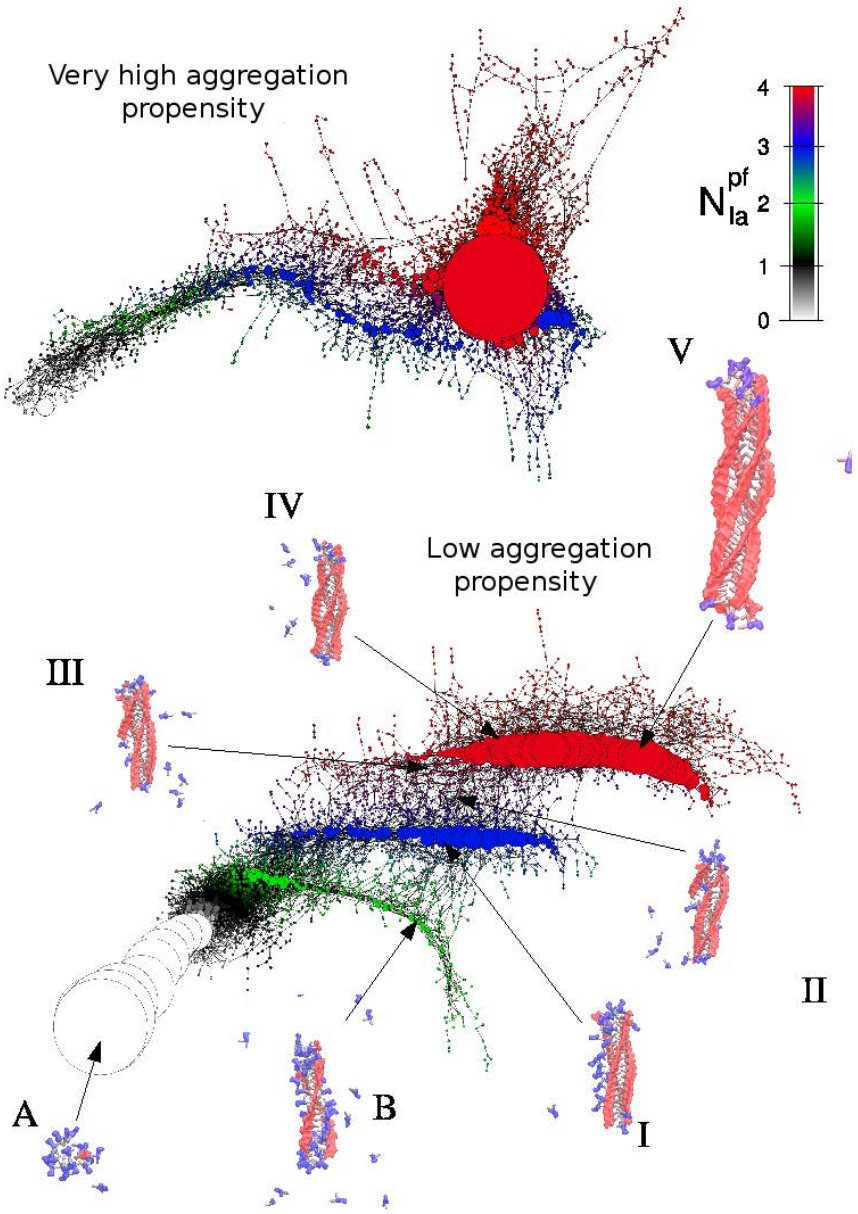

FIG. 7. Aggregation state network. The size of the largest aggregate N_{la} and its number of protofilaments N_{la}^{pf} were used to cluster all simulation snapshots into states (i.e., nodes of the network). The size and the colour of nodes correspond to the statistical weight and the number of protofilaments N_{la}^{pf}, respectively. Links are direct transitions within 0.5 ns of Langevin dynamics. Note the much higher heterogeneity of protofibrillar intermediates for the β-unstable (dE = -2.5 kcal/mol, bottom) as compared to the β-stable (dE = -1.5 kcal/mol, top) model. The insets show (proto)fibrillar structures that are representative of each region of the aggregation state network. In these structures, monomers in the amyloid-competent conformer β and amyloid-protected conformer π are in red and blue, respectively. Furthermore, hydrophobic spheres are gray and hydrophlic spheres are not shown for visual clarity. Reprinted from[50] with permission by Elsevier.

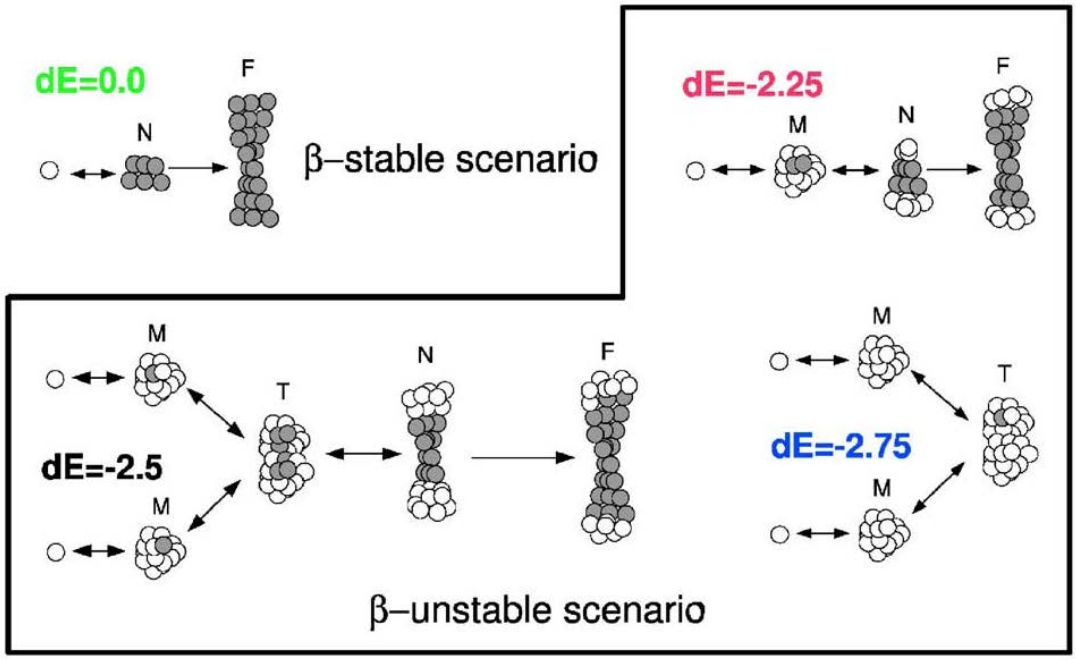

FIG. 8. Observed nucleation scenarios of the CGF peptide model. Black and white circles represent the amyloid-competent conformer β and amyloid-protected conformer π, respectively. CGF peptides with high values of amyloidogenic tendency nucleate without intermediates, while poorly amyloidogenic CGF peptides can nucleate either through micelle-sized oligomers (dE = -2.25 kcal/mol) or transient oligomers larger than a micelle (dE = -2.5 kcal/mol). A further stabilization (dE = -2.75 kcal/mol) of the protected state prevents fibril formation within the simulation time of about 20 μs. M, micelle; N, nucleus; T, transient oligomer; F, fibril. Reprinted from[37] with permission by Elsevier.

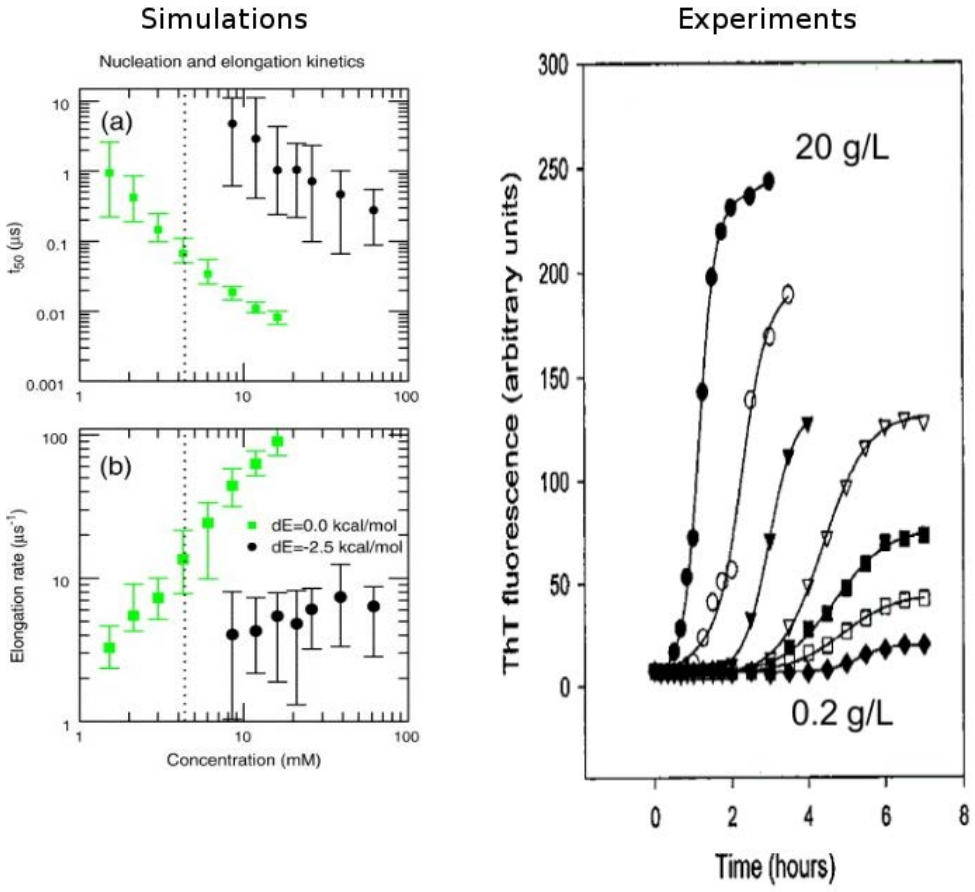

FIG. 9. Influence of peptide concentration on aggregation kinetics. (Left) Effect of concentration on the lag phase time t_{50} (a) and elongation rate (b) for low and high values (dE = -2.5 kcal/mol, black circles; dE = 0.0 kcal/mol, green squares, respectively) of the amyloidogenic tendency. The symbols represent the average value calculated from 15 simulations for dE = -2.5 kcal/mol and ten simulations for dE = 0.0 kcal/mol. The error bars represent the minimum and the maximum values. The vertical dotted line indicates the critical concentration of micelle formation. (Right) Influence of the initial monomeric concentration on the kinetics of insulin fibril formation as measured by Thioflavin T fluorescence[58]. Note that the higher the concentration of monomeric insulin is at the beginning of the experiments, the shorter is the lag phase and the faster is the elongation rate. Reprinted from[37] (left) and[58] (right) with permission by Elsevier (left) and American Chemical Society (right).

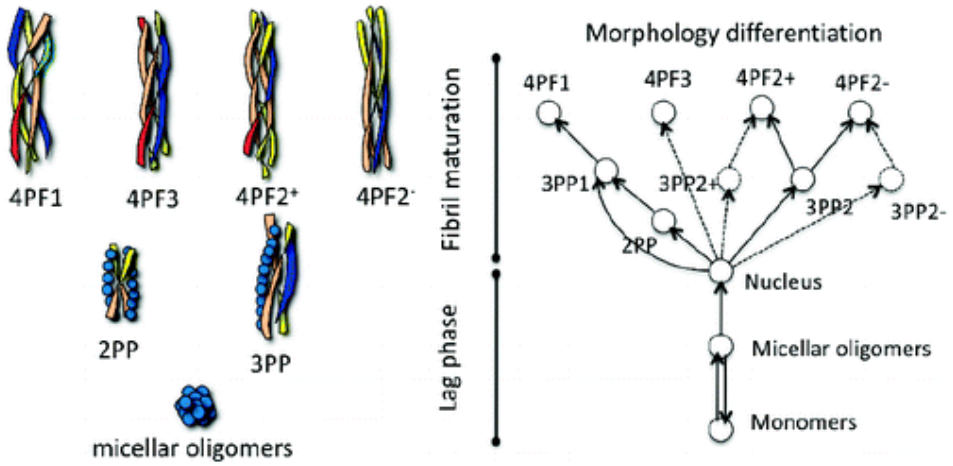

FIG. 10. Morphology differentiation and kinetic control of fibril polymorphism. (Left) Morphologies of mature fibrils and prefibrillar species. (Top) Mature fibrils display a 4-protofilament structure (4PF). The 4PF morphologies have different orientation of the protofilaments, organization of up and down protofilaments, and thickness of the fibril. (Bottom) The prefibrillar species are: the micellar oligomers M, consisting of π-monomers (blue beads) aggregated through hydrophobic forces; the 2-protofilament protofibril (2PP), and the 3-protofilament protofibril (3PP), which are early stages of fibril maturation, where the π-monomers are deposited onto the lateral surface of the fibril, and the β-monomers make up the protofilaments (colored ribbons). (Right) Branched tree illustration of the morphology differentiation process as observed in the simulations. Reprinted from[64] with permission by American Chemical Society.

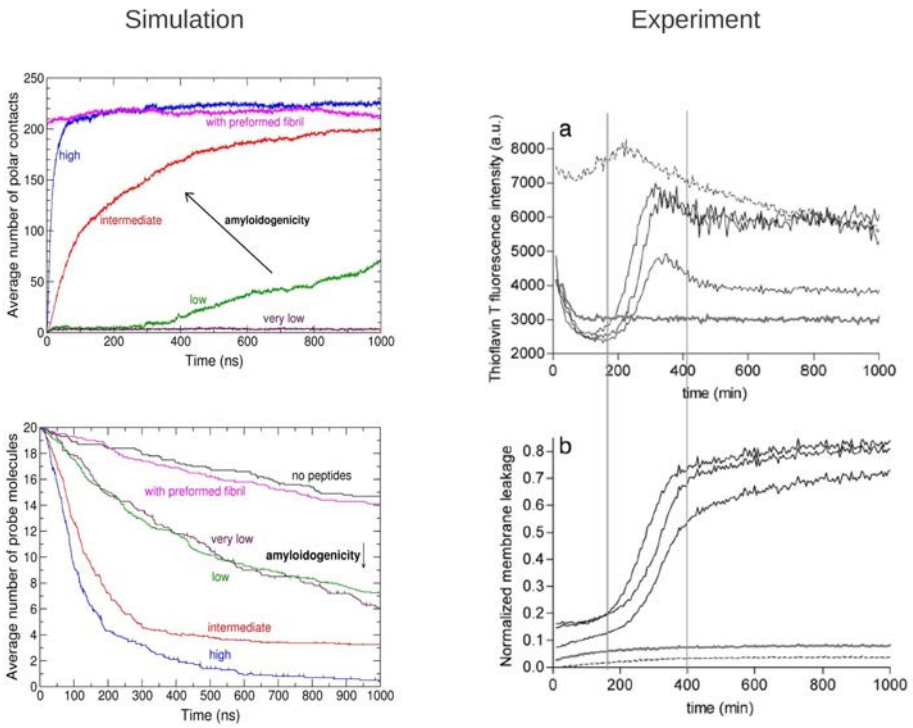

FIG. 11. Comparison of CGF model simulations and experimental data on fibril formation in the presence of lipid vesicles. (Left) Simulation results. (Left, top) Influence of peptide amyloidogenicity on fibril growth kinetics and vesicle leakage. A single parameter, the energy difference between amyloid-competent and amyloid-protected conformations of the peptides, is varied in different simulations to tune amyloidogenicity. Time series of the average number of ordered polar contacts between monomers (corresponding to the degree of fibrillation). (Left, bottom) Average number of probes inside the vesicle, in the absence (black) or presence (colors) of peptides, and for simulations where a preformed fibril was used instead of dispersed peptides. (Right) Experimental data: Effect of human islet amyloid polypeptide (hIAPP) fibril growth on membrane leakage[69]. Thioflavin T fluorescence intensity (Right, top) and induced membrane leakage (Right, bottom) of three hIAPP samples (black curves), together with representative traces for mouse IAPP variant which is known to be non-toxic amyloid polypeptide (gray lines) and preformed hIAPP fibrils (dashed lines) are shown. The two vertical lines are shown to facilitate comparison of the kinetic traces in top and bottom panel. Reprinted from[73] (left) and[69] (right) with permission by Elsevier and by Copyright 2008 National Academy of Sciences, U.S.A., respectively.

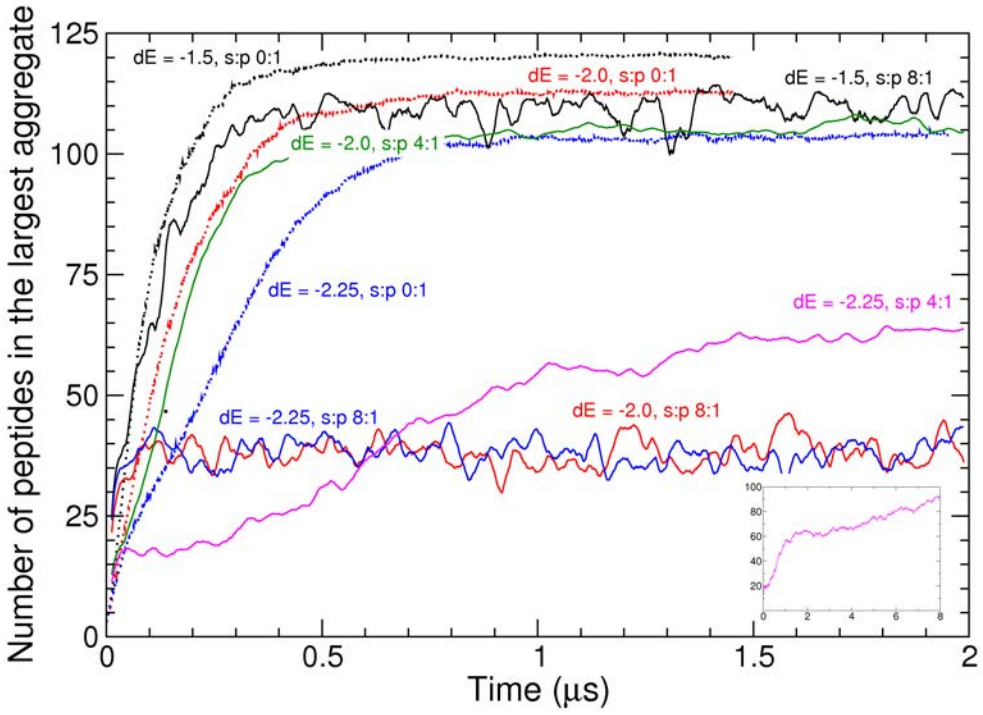

FIG. 12. Amyloid aggregation in the presence and absence of surfactants. The number of peptides in the largest aggregate is averaged over 20 runs at each simulation condition, i.e., for each value of aggregation propensity (dE) and each surfactant/peptide concentration ratio (s:p). Free peptides display fast aggregation without any noticeable lag phase. At surfactant:peptide ratio of 4:1, peptides aggregate into fibrils, but aggregation is much slower for peptides with low amyloidogenicity (see the inset for dE = -2.25 and surfactant:peptide ratio of 4:1, extended to 8 μs). At a surfactant:peptide ratio of 8:1, aggregation is completely inhibited for dE = -2.0 and -2.25 kcal/mol, while highly amyloidogenic peptides (dE = -1.5 kcal/mol) are barely affected.

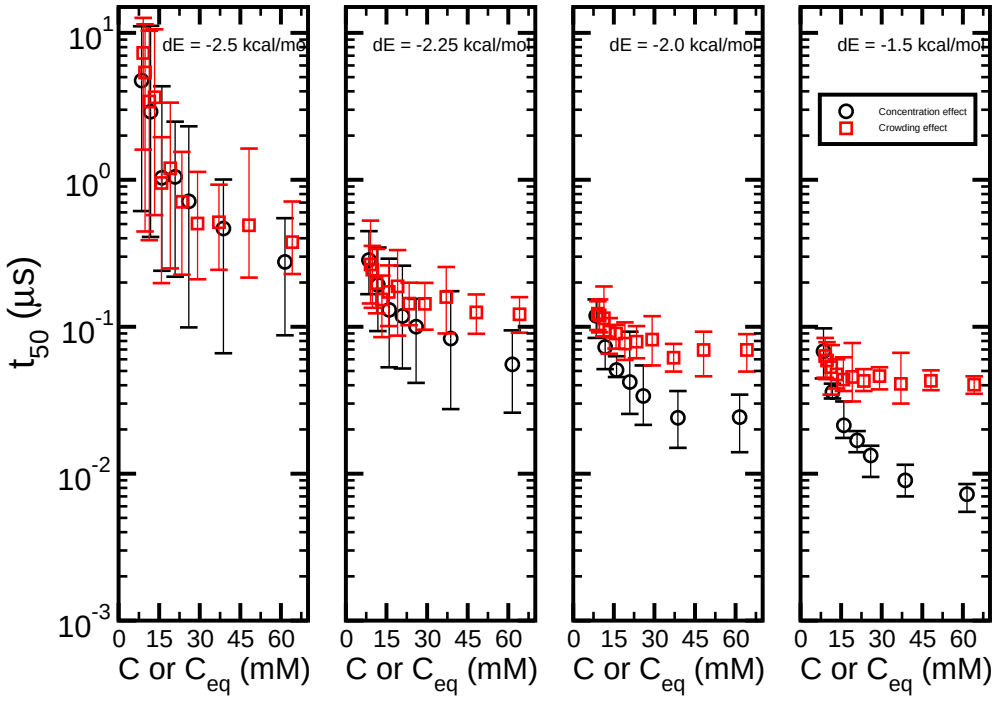

FIG. 13. The deviation of aggregation kinetics between crowded and bulk conditions depends on the amyloidogenicity. The time t_{50}, at which the growing fibril has reached 50% of the polar contacts of the mature fibril, is shown as a function of concentration. Black circles are t_{50} values calculated at different peptide concentrations in the absence of crowders, while red squares are t_{50} values at different equivalent concentrations C_{eq} obtained by varying the number of crowders. Symbols represent the average value of 10 independent runs and the error bars are the minimum and maximum values. Reprinted from[81] with permission by American Chemical Society.